

IRREGULARITY REFLECTION NEURAL NETWORK FOR TIME SERIES FORECASTING

Anonymous authors

Paper under double-blind review

ABSTRACT

Time series forecasting is a long-standing challenge in a variety of industries, and deep learning stands as the mainstream paradigm for handling this forecasting problem. With recent success, representations of time series components (e.g., trend and seasonality) are also considered in the learning process of the models. However, the residual remains under explored due to difficulty in formulating its inherent complexity. In this study, we propose a novel Irregularity Reflection Neural Network (IRN) that reflect the residual for the time series forecasting. First, we redefine the residual as the irregularity and express it as a sum of individual, short regular waves considering the Fourier series in a micro perspective. Second, we design a module, based on the convolutional architectures to mimic the variables of the derived irregularity representation, named Irregularity Representation Block (IRB). IRN comprises IRB on top of a forecasting model to learn the irregularity representation of time series. Extensive experiments on multiple real-world datasets demonstrate that IRN outperforms the state-of-the-art benchmarks in time series forecasting tasks.

1 INTRODUCTION

Owing to the ubiquitous computing systems, time series is available in a wide range of domains including traffic (Chen et al., 2001), power plant (Gensler et al., 2016), stock market indices (Song et al., 2021), and so on (Liu et al., 2015; Duan et al., 2021). Spontaneously, interests in time series forecasting have grown, and as a result, an intensive research for a more accurate prediction.

In recent literature, many deep learning models have been favored for forecasting problems (Lim & Zohren, 2021). Recurrent Neural Network (RNN) and its extensions such as Long Short-Term Memory (LSTM) (Hochreiter & Schmidhuber, 1997) and Gated Recurrent Unit (GRU) (Chung et al., 2014) are popular choices for analyzing long sequences. Nevertheless, these models tend to be restricted in handling multivariate time series. As a powerful alternative, Convolution Neural Networks (CNNs) has been introduced to capture overall characteristics of time series through parallel calculations and filter operations. Building on the success in forecasting task, CNN-based models have been proposed according to the type of time series data. Temporal Convolutional Network (TCN) was applied to audio datasets (Oord et al., 2016), whereas Graph Convolutional Network (GCN) was utilized in the time series with graph characteristics (e.g., human skeleton-based action recognition (Zhang et al., 2020) and traffic dataset (Bai et al., 2020)). The attention models have also been applied to emphasize the specific sequence data that are primarily referenced when making the predictions (Liu et al., 2021b).

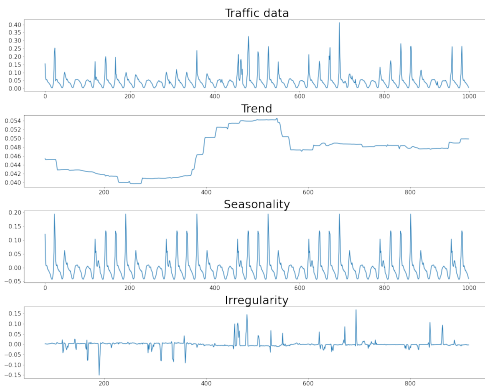


Figure 1: The Traffic data and its time series components (i.e., trend, seasonality, and irregularity).

Despite the great efforts made, forecasting performance has room for further improvement as aforementioned models learn feature representations directly from complex real-world time series, often overlooking essential information. Recently, incorporating representations of time series components (e.g., trend, seasonality) used in conventional econometric approaches have shown to lead to better performances of the learning models. For instance, N-BEATS (Oreshkin et al., 2019), Autoformer (Wu et al., 2021), and CoST (Woo et al., 2022) reflected the trend and seasonality of the time series and achieved improvements. However, as shown in Figure 1, time series also include the irregularity that is not accounted by the trend and seasonality, and is yet under explored (Woo et al., 2022).

To address this challenge, we show how to deal with the irregularity of the time series data to improve the forecasting performance of the deep learning models. To this end, we represent the irregularity into an encodable expression on basis of Fourier series viewed from a micro perspective. The derived representation is encoded using convolutional architectures, and named as Irregularity Representation Block (IRB). Then, IRB embedded on a base model builds the Irregularity Reflection Neural Network (IRN). We demonstrate that IRN outperforms existing state-of-the-art forecasting models on eleven popular real-world datasets.

2 RELATED WORK

2.1 DEEP LEARNING FOR TIME SERIES FORECASTING

Sequential deep learning models such as RNN, LSTM, and GRU have long been used for time series forecasting (Elman, 1990; Hochreiter & Schmidhuber, 1997; Chung et al., 2014). Although effective in capturing the temporal dependencies of time series, RNN-based models neglect the correlations in-between time series. To tackle this issue, Liu et al. (2020) propose a dual-stage two-phase (DSTP) to extract the spatial and temporal features. Shi et al. (2015) present convLSTM replacing the states of LSTM block with convolutional states. Another limitation of the sequential models are that the discrepancy between ground truth and prediction is accumulated over time as predictions are referred to predict further into the future (Liu et al., 2021a).

More recent works have demonstrated that CNNs can be applied in multivariate time series problems as well. Ravi et al. (2016) introduce the 1D convolution for human activity recognition, whereas Zhao et al. (2017) suggest the use of 2D convolution. CNN models are parallelizable, and hence show following advantages: the consideration of the correlation between variates and the prevention of error accumulation (Liu et al., 2019). A downside is the limited receptive field when predicting long sequences due to the increasing number of the parameters (Zhao et al., 2017). Wang et al. (2019) tackle this challenge by decomposing the long sequences according to long, short and closeness.

CNN-based models have received increasing attention to enhance the forecasting performance. For example, the dilated casual convolutional layer is used to increase the receptive field by down-sampling and improve long sequences prediction (Sen et al., 2019; Oord et al., 2016). Another approach is Graph Convolutional Network (GCN), that analyzes the relation between nodes with specific position and edge relation, especially in traffic data (Fang et al., 2021; Song et al., 2020) and human body skeleton data (Yoon et al., 2022; Chen et al., 2021). Attention-based models have also been adopted (Liu et al., 2019) and further developed into Transformer (Zhou et al., 2021; Liu et al., 2021b). However, these approaches do not take into account the characteristics of time series such as trend, seasonality and irregularity.

2.2 REFLECTING THE REPRESENTATIVE COMPONENTS OF TIME SERIES

Considerable studies on time series analysis have relied on the decomposition of time series into non-random components. For instance, DeJong et al. (1992) conducted analysis on the trends of the macroeconomic time series as well as Lee & Shen (2009) emphasized the importance of obtaining significant trend relationship in linear time complexity. Jonsson & Eklundh (2002) extracted and analyzed the seasonality of the time series data and Taylor & Letham (2018) considered both trend and seasonality. When extracting these non-random components, a non-stationary time series becomes stationary, meaning time-independent. As conventional statistical methods such as ARIMA (Autoregressive Integrated Moving Average) (Williams & Hoel, 2003) and GP (Gaussian Process)

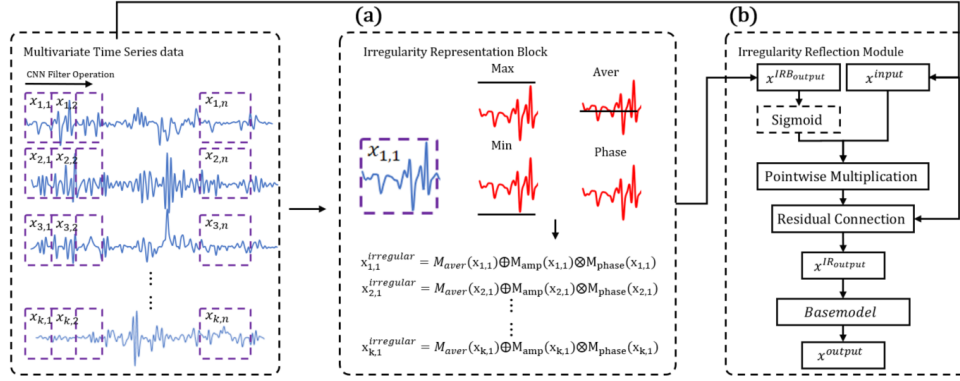


Figure 2: An overview of IRN framework. In IRN, (a) IRB extracts the irregularity feature from the input sequences and (b) Irregularity Reflection module conducts the time series forecasting.

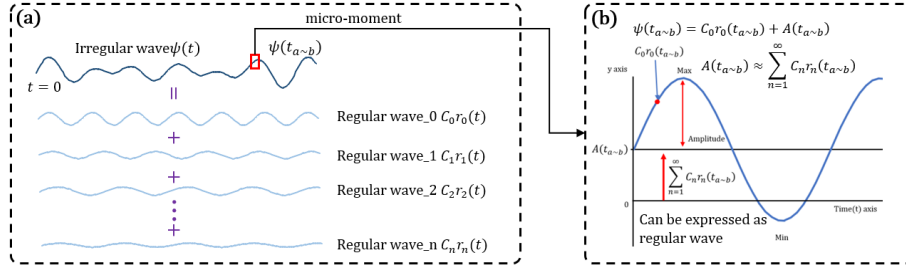


Figure 3: (a) The irregular wave $\psi(t)$ consisting of multiple regular waves and (b) the irregular wave from a micro perspective $\psi(t_{a~b})$.

(Van Der Voort et al., 1996) perform better on stationary data (Cheng, 2018), differentiation for stationarity has been conducted (Atique et al., 2019). As such, extraction of the representative time series components for forecasting problems has been a major research topic (Brockwell & Davis, 2009; Cleveland et al., 1990).

Recently, direct learning from input sequences of the deep forecasting models is regarded to be enough, thereupon researchers focus on how to incorporate the components of time series in the learning process. For instance, Oreshkin et al. (2019) proposed a hierarchical doubly residual topology as the interpretable architecture to extract time series representations: trend, and seasonality. Wu et al. (2021) proposed a transformer-based model which decomposes and reflects the trend and seasonality by using auto-correlation mechanism. Woo et al. (2022) introduced disentangled Seasonal-Trend Representation Learning by using the independent mechanisms. They devised disentanglers for the trend and seasonal features, mainly composed of a discrete Fourier transform to map the intermediate features to frequency domain. These studies successfully reflect representations of trend and seasonality which are the time dependent value, and improve forecasting performances. However, the irregularity, which cannot be explained by the trend or seasonality and is the time independent value, is not sufficiently addressed. In this paper, we build and reflect the irregularity representation to complement the previous researches in forecasting tasks.

3 METHODOLOGY

In this section, we discuss how to reinterpret the irregularity of the time series in term of Fourier series, extract and reflect the irregularity representation using convolutional architectures. Our proposed model IRN is shown in Figure 2.

3.1 THEORETICAL APPROACH

A time series is generally in the form of an irregularity. Hence, its representation is essential for time series forecasting. Among many existing approaches to represent irregularity, Fourier series is perhaps the most widely used. Fourier series approximates irregularity by the linear superposition of multiple regular waves with varying height, period, and direction as depicted in Figure 3 (a) (Bloomfield, 2004). The irregularity $\psi(t)$ can be expressed as:

$$\psi(t) = \sum_{n=0}^{\infty} C_n r_n(t) \quad (1)$$

where $r_n(t)$ is n-th regular wave, C_n is the coefficient of $r_n(t)$, t is the time. The concept of infinity in Equation 1 is challenging for the learning model to handle. Therefore, we reinterpret $\psi(t)$ into an encodable equation by viewing it at the micro level. When the irregularity $\psi(t)$ in the time domain is observed at the moment $t_{a\sim b}$, it can be interpreted as a regular wave $\psi(t_{a\sim b})$ with a vertical shift, which is the average value of the regular waves. Under this concept, Equation 1 is rewritten as:

$$\psi(t_{a\sim b}) = C_0 r_0(t_{a\sim b}) + \sum_{n=1}^{\infty} C_n r_n(t_{a\sim b}) \quad (2)$$

where $C_0 r_0(t_{a\sim b})$ is the representative regular wave characteristic. $C_0 r_0(t_{a\sim b})$ is the regular wave with a mean of 0 without vertical shift. The representative regular wave $r_0(t_{a\sim b})$ oscillates between the constant maximum and minimum values in a period of time and can be defined as $Amplitude \times \sin(\omega \times t_{a\sim b})$, where the angular velocity ω is constant due to the periodicity of the wave, $\omega \times t_{a\sim b}$ is denoted as the angle θ of $r_0(t_{a\sim b})$, and $\sin(\omega \times t_{a\sim b})$ is the phase of $r_0(t_{a\sim b})$. $Amplitude$ is calculated with the peaks of the wave. Accordingly, the representative regular wave $r_0(t_{a\sim b})$ can be rewritten as:

$$r_0(t_{a\sim b}) = \frac{\max(t_{a\sim b}) - \min(t_{a\sim b})}{2} \times \sin(\theta(t_{a\sim b})) \quad (3)$$

where $\sin(\theta(t_{a\sim b}))$ is the phase of $r_0(t_{a\sim b})$ at $t_{a\sim b}$. Therefore, $C_0 r_0(t_{a\sim b})$ in Equation 2 is redefined by referring to Equation 3. The remaining infinity term $\sum_{n=1}^{\infty} C_n r_n(t_{a\sim b})$ in Equation 2 corresponds to the vertical shift and can be expressed as the average value $A(t_{a\sim b})$ of $\psi(t_{a\sim b})$ as depicted in Figure 3 (b). The representative regular wave $C_0 r_0(t_{a\sim b})$ and the average value $\sum_{n=1}^{\infty} C_n r_n(t_{a\sim b})$ convert Equation 2 into:

$$\psi(t_{a\sim b}) \approx A(t_{a\sim b}) + \frac{\max(t_{a\sim b}) - \min(t_{a\sim b})}{2} \times \sin(\theta(t_{a\sim b})) \quad (4)$$

When the regular waves are sequentially connected, we obtain the irregularity $\psi(t)$ consisting of the regular waves that change with time $t_{a\sim b}$. We redefine the Equation 4 as follows:

$$\psi(t) \approx A(t) + \frac{\max(t) - \min(t)}{2} \times \sin(\theta(t)) \quad (5)$$

where $\frac{\max(t) - \min(t)}{2}$ is the amplitude of the regular wave $C_0 r_0(t_{a\sim b})$ at $t_{a\sim b}$, $\sin(\theta(t))$ is the phase of $C_0 r_0(t_{a\sim b})$ at $t_{a\sim b}$, and $A(t)$ is the average which is the sum of remained regular waves $\sum_{n=1}^{\infty} C_n r_n(t_{a\sim b})$ at $t_{a\sim b}$. According to Equation 5, the irregularity $\psi(t)$ can be represented by the combinations of the minimum, maximum, average, and phase values.

3.2 IRREGULARITY REPRESENTATION BLOCK

Based on Equation 5, the irregularity is encoded to incorporate into deep learning models. In this paper, convolutional architectures are adopted since convolutional layers allow the parallel prediction

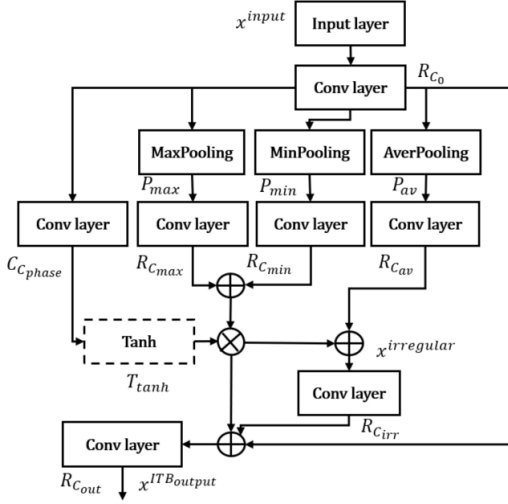


Figure 4: Architecture of the Irregularity Representation Block.

as well as analysis of relations existing in multivariate time series through filter operations. We input the multivariate time series $x^{input} \in \mathbb{R}^{T \times d}$, where T is a look-back window of fixed length, and d is the number of variates. Our model stacks multiple convolution layers with the RELU activation function, a dilation filter and same padding. The RELU activation increases the model complexity through space folding (Montufar et al., 2014), and the dilation operation helps expand the receptive fields (Oord et al., 2016). The convolution layer extracts the feature that has the same size of the x^{input} through the same padding. Accordingly, Equation 5 is transformed into

$$x^{irregular} = A(x^{input}) \oplus \frac{\max(x^{input}) - \min(x^{input})}{2} \otimes \sin(\theta(x^{input})) \quad (6)$$

where \oplus is the pointwise summation, \otimes is the pointwise multiplication, and $x^{irregular}$ is the irregularity. Through this transformation, the $x^{irregular}$ is converted from time dependent to data dependent and the main operations (i.e., $A()$, $\max()$, $\min()$, and $\sin(\theta())$) are expressed by using the convolution layers and pooling layers which extract the average, the maximum, the minimum, and the phase value from x^{input} under microscopic perspective condition. The main operations are encoded like Figure 4 as follows:

$$M_{aver}(x^{input}) = R_{C_{av}}(P_{av}(R_{C_0}(x^{input}))) \approx A(x^{input}) \quad (7)$$

$$M_{amp}(x^{input}) = \frac{R_{C_{max}}(P_{max}(R_{C_0}(x^{input}))) - R_{C_{min}}(P_{min}(R_{C_0}(x^{input})))}{2} \approx \frac{\max(x^{input}) - \min(x^{input})}{2} \quad (8)$$

$$M_{phase}(x^{input}) = T_{tanh}(C_{C_{phase}}(R_{C_0}(x^{input}))) \approx \sin(\theta(x^{input})) \quad (9)$$

where P_{max} , P_{min} , and P_{av} are the max, min, and average pooling operations, respectively. C is the convolution layer without activation, R is C with the RELU activation and T_{tanh} is the hyperbolic tangent(tanh) activation. Through this process, the average, amplitude, and phase values in Equation 6 are converted to trainable values. To extract the representation of the average value from x^{input} , we stack the 2D convolution filter and the 2D average pooling as in Equation 7. To decompose the representation of the amplitude from x^{input} , we construct the structure same as Equation 8 with the 2D max and min pooling. To obtain the representation of the adaptive phase value using x^{input} under microscopic aspect condition, referring to the Equation 9, we use the tanh activation after convolution layer. Consequently, these operations(i.e., $M_{aver}(x^{input})$, $M_{amp}(x^{input})$, and $M_{phase}(x^{input})$) extract the average, amplitude, and phase values from x^{input} , and we redefine Equation 6 as follows:

$$x^{irregular} = M_{aver}(x^{input}) \oplus M_{amp}(x^{input}) \otimes M_{phase}(x^{input}) \quad (10)$$

To consider the $x^{irregular}$ value, we apply the residual stacking principle which enables complex interpretation by combining features in a hierarchical form for each step (Oreshkin et al., 2019). Therefore, we design the IRB architecture as follows:

$$R_{C_{out}}(R_{C_{irr}}(x^{irregular}) \oplus R_{C_0}(x^{input}) \oplus M_{amp}(x^{input}) \otimes M_{phase}(x^{input})) \quad (11)$$

The output of IRB $x^{IRB_{output}}$ is the representation of the irregularity which considers the average, amplitude, phase, and input components. Furthermore, these components are trainable values because they consist of the convolution layers.

3.3 IRREGULARITY REFLECTION NEURAL NETWORK

IRN consists of IRB and a irregularity reflection module as in Figure 2. For the forecasting of this study, a recent model that reflects trend and seasonality, known as SCIInet (Liu et al., 2021a) is used as the base model. The $x^{IRB_{output}}$ is passed to the base model through the irregularity reflection module.

$$x^{IR_{output}} = S_{sig}(x^{IRB_{output}}) \otimes x^{input} \oplus x^{input} \quad (12)$$

where $x^{IR_{output}}$ is the output of IRN and S_{sig} is the sigmoid activation. The pointwise multiplication is applied to emphasize the irregularity of the x^{input} by using the $x^{IRB_{output}}$ with S_{sig} . If we use the $x^{IRB_{output}}$ as the input value of the time series model, some information (e.g., trend, seasonality) can be omitted. To alleviate this problem, we preserve the original information by residual connection, which also prevents the gradient vanishing (He et al., 2016).

Table 1: Summary of datasets and evaluation metrics used for time series forecasting.

Type	Dataset	Variates	Timesteps	Granularity	Start time	Metrics	Train/Val/Test
ETT (Zhou et al., 2021)	ETTh1	7	17420	1 hour	7/1/2016	MSE	12/4/4
	ETTh2		69680	15 min		MAE	
	ETTm1						
PEMS (Chen et al., 2001)	PEMS03	358	26209	5 min	5/1/2012 7/1/2017 5/1/2017 3/1/2012	MAE	6/2/2
	PEMS04	307	16992			MAPE	
	PEMS07	883	28224			RMSE	
	PEMS08	170	17856				
Solar,		137	52560	10 min	2016		
Traffic,		862	17544	1 hour	2015	RSE	6/2/2
Electricity,		321	26304		2012	CORR	
Exchange-rate (Lai et al., 2018)		8	7588	1 day	1990		

Table 2: Multivariate forecasting performance of IRN and baseline models on the ETT datasets. Best results are highlighted in bold.

Model	Metrics	ETTh1					ETTh2					ETTm1				
		24	48	168	336	720	24	48	168	336	720	24	48	96	288	672
LogTrans	MSE	0.686	0.766	1.002	1.362	1.397	0.828	1.806	4.07	3.875	3.913	0.419	0.507	0.768	1.462	1.669
	MAE	0.604	0.757	0.846	0.952	1.291	0.75	1.034	1.681	1.763	1.552	0.412	0.583	0.792	1.32	1.461
Reformer	MSE	0.991	1.313	1.824	2.117	2.415	1.531	1.871	4.66	4.028	5.381	0.724	1.098	1.433	1.82	2.187
	MAE	0.754	0.906	1.138	1.28	1.52	1.613	1.735	1.846	1.688	2.015	0.607	0.777	0.945	1.094	1.232
TCC	MSE	0.766	0.825	0.982	1.099	1.267	1.154	1.579	3.456	3.184	3.538	0.502	0.645	0.675	0.758	0.854
	MAE	0.629	0.657	0.731	0.786	0.859	0.838	0.983	1.459	1.42	1.523	0.478	0.559	0.583	0.633	0.689
TST	MSE	0.735	0.8	0.973	1.029	1.02	0.994	1.159	2.609	2.824	2.684	0.471	0.614	0.645	0.749	0.857
	MAE	0.633	0.671	0.768	0.797	0.798	0.779	0.85	1.265	1.337	1.334	0.491	0.56	0.581	0.644	0.709
CPC	MSE	0.728	0.774	0.92	1.05	1.16	0.551	0.752	2.452	2.664	2.863	0.478	0.641	0.707	0.781	0.88
	MAE	0.6	0.629	0.714	0.779	0.835	0.572	0.684	1.213	1.304	1.399	0.459	0.55	0.593	0.644	0.7
Triplet	MSE	0.942	0.975	1.135	1.187	1.283	1.285	1.455	2.175	2.007	2.157	0.689	0.752	0.744	0.808	0.917
	MAE	0.729	0.746	0.825	0.859	0.916	0.911	0.966	1.155	1.101	1.139	0.592	0.624	0.623	0.662	0.72
MoCo	MSE	0.623	0.669	0.82	0.981	1.138	0.444	0.613	1.791	2.241	2.425	0.458	0.594	0.621	0.7	0.821
	MAE	0.555	0.586	0.674	0.755	0.831	0.495	0.595	1.034	1.186	1.292	0.444	0.528	0.553	0.606	0.674
TNC	MSE	0.708	0.749	0.884	1.02	1.157	0.612	0.84	2.359	2.782	2.753	0.522	0.695	0.731	0.818	0.932
	MAE	0.592	0.619	0.699	0.768	0.83	0.592	0.716	1.213	1.349	1.394	0.472	0.567	0.595	0.649	0.712
Informer	MSE	0.577	0.685	0.931	1.128	1.215	0.72	1.457	3.489	2.723	3.467	0.323	0.494	0.678	1.056	1.192
	MAE	0.549	0.625	0.752	0.873	0.896	0.665	1.001	1.515	1.34	1.473	0.369	0.503	0.614	0.786	0.926
TS2Vec	MSE	0.59	0.624	0.762	0.931	1.063	0.423	0.619	1.845	2.194	2.636	0.453	0.592	0.635	0.693	0.782
	MAE	0.531	0.555	0.639	0.728	0.799	0.489	0.605	1.074	1.197	1.37	0.444	0.521	0.554	0.597	0.653
SCInet	MSE	0.341	0.368	0.451	0.502	0.583	0.188	0.279	0.505	0.618	1.074	0.126	0.169	0.191	0.365	0.713
	MAE	0.379	0.395	0.457	0.497	0.56	0.288	0.358	0.504	0.56	0.761	0.229	0.274	0.291	0.415	0.604
Pyraformer	MSE	-	-	0.808	0.945	1.022	-	-	-	-	-	-	-	0.48	0.754	0.857
	MAE	-	-	0.683	0.766	0.806	-	-	-	-	-	-	-	0.486	0.659	0.707
Cost	MSE	0.386	0.437	0.643	0.812	0.97	0.447	0.699	1.549	1.749	1.971	0.246	0.331	0.378	0.472	0.62
	MAE	0.379	0.464	0.582	0.679	0.771	0.502	0.637	0.982	1.042	1.092	0.329	0.386	0.419	0.486	0.574
Autoformer	MSE	0.384	0.392	0.49	0.505	0.498	0.261	0.312	0.457	0.471	0.474	0.383	0.454	0.481	0.634	0.606
	MAE	0.425	0.419	0.481	0.484	0.5	0.341	0.373	0.455	0.475	0.484	0.403	0.453	0.463	0.528	0.542
IRN	MSE	0.314	0.343	0.429	0.467	0.49	0.182	0.241	0.437	0.51	1.07	0.124	0.143	0.184	0.342	0.559
	MAE	0.361	0.368	0.432	0.474	0.501	0.27	0.314	0.453	0.498	0.745	0.223	0.249	0.28	0.398	0.522

4 EXPERIMENTS

We conduct experiments on 11 real-world time series datasets and compare the performance with the latest baselines. We analyze the circumstances in which proposed IRB improves the forecasting performance. We refer base model (Liu et al., 2021a) for the experiment settings. Due to page limits, the implementation details including the loss function, datasets, and metrics are reported in the Appendix.

4.1 DATASET

Experiments are conducted on following time series datasets: Electricity Transformer Temperature (Zhou et al., 2021), PEMS (Chen et al., 2001), Solar, Traffic, Electricity, Exchange-rate (Lai et al., 2018). The datasets, experiment settings, and metrics are summarized in Table 1.

Table 3: Univariate forecasting performance of IRN and baseline models on the ETT datasets. Best results are highlighted in bold.

Model	Metrics	ETTh1					ETTh2					ETTm1				
		24	48	168	336	720	24	48	168	336	720	24	48	96	288	672
N-BEAT	MSE	0.042	0.065	0.106	0.127	0.269	0.078	0.123	0.244	0.27	0.281	0.031	0.056	0.095	0.157	0.207
	MAE	0.156	0.2	0.255	0.284	0.422	0.21	0.271	0.393	0.418	0.432	0.117	0.168	0.234	0.311	0.37
Informer	MSE	0.098	0.158	0.183	0.222	0.269	0.093	0.155	0.232	0.263	0.277	0.03	0.069	0.194	0.401	0.512
	MAE	0.247	0.319	0.346	0.387	0.435	0.24	0.314	0.389	0.417	0.431	0.137	0.203	0.372	0.554	0.644
TCC	MSE	0.053	0.074	0.133	0.161	0.176	0.111	0.148	0.225	0.232	0.242	0.026	0.045	0.072	0.158	0.239
	MAE	0.175	0.209	0.284	0.32	0.343	0.255	0.298	0.374	0.385	0.397	0.122	0.165	0.211	0.318	0.398
TST	MSE	0.127	0.202	0.491	0.526	0.717	0.134	0.171	0.261	0.269	0.278	0.048	0.064	0.102	0.172	0.224
	MAE	0.284	0.362	0.596	0.618	0.76	0.281	0.321	0.404	0.413	0.42	0.151	0.183	0.231	0.316	0.366
CPC	MSE	0.076	0.104	0.162	0.183	0.212	0.109	0.152	0.251	0.238	0.234	0.018	0.035	0.059	0.118	0.177
	MAE	0.217	0.259	0.326	0.351	0.387	0.251	0.301	0.392	0.388	0.389	0.035	0.142	0.188	0.271	0.332
Triplet	MSE	0.13	0.145	0.173	0.167	0.195	0.16	0.181	0.214	0.232	0.251	0.071	0.084	0.097	0.13	0.16
	MAE	0.289	0.306	0.336	0.333	0.368	0.316	0.339	0.372	0.389	0.406	0.18	0.206	0.23	0.276	0.315
MoCo	MSE	0.04	0.063	0.122	0.144	0.183	0.095	0.13	0.204	0.206	0.206	0.015	0.027	0.041	0.083	0.122
	MAE	0.151	0.191	0.268	0.297	0.347	0.234	0.279	0.36	0.364	0.369	0.091	0.122	0.153	0.219	0.268
TNC	MSE	0.057	0.094	0.171	0.192	0.235	0.097	0.131	0.197	0.207	0.207	0.19	0.036	0.054	0.098	0.136
	MAE	0.184	0.239	0.329	0.357	0.408	0.238	0.281	0.354	0.366	0.37	0.103	0.142	0.178	0.244	0.29
TS2Vec	MSE	0.039	0.062	0.142	0.16	0.179	0.091	0.124	0.198	0.205	0.208	0.016	0.028	0.045	0.095	0.142
	MAE	0.151	0.189	0.291	0.316	0.345	0.23	0.274	0.355	0.364	0.371	0.093	0.126	0.162	0.235	0.29
SCIInet	MSE	0.031	0.051	0.081	0.094	0.176	0.07	0.102	0.157	0.177	0.253	0.019	0.045	0.072	0.117	0.18
	MAE	0.132	0.173	0.222	0.242	0.343	0.194	0.242	0.311	0.34	0.403	0.088	0.143	0.198	0.266	0.328
CoST	MSE	0.04	0.06	0.097	0.112	0.148	0.079	0.118	0.189	0.206	0.214	0.015	0.025	0.038	0.077	0.113
	MAE	0.152	0.186	0.236	0.258	0.306	0.207	0.259	0.339	0.36	0.371	0.088	0.117	0.147	0.209	0.257
IRN	MSE	0.03	0.045	0.078	0.091	0.168	0.067	0.093	0.154	0.172	0.235	0.018	0.043	0.07	0.116	0.151
	MAE	0.131	0.163	0.218	0.241	0.329	0.189	0.232	0.31	0.337	0.392	0.087	0.141	0.196	0.264	0.301

Table 4: Forecasting performance of IRN and baseline models on PEMS datasets. Best results are highlighted in bold.

Model	PEMS03			PEMS04			PEMS07			PEMS08		
	MAE	RMSE	MAPE (%)	MAE	RMSE	MAPE (%)	MAE	RMSE	MAPE (%)	MAE	RMSE	MAPE (%)
LSTM	21.33	35.11	21.33	25.14	39.59	20.33	29.98	42.84	15.33	22.2	32.06	15.32
TCN	18.87	32.24	18.63	22.81	36.87	14.31	30.53	41.02	13.88	21.42	34.03	13.09
DCRNN	18.18	30.31	18.91	24.7	38.12	17.12	28.3	38.58	11.66	17.86	27.83	11.45
STGCN	17.49	30.12	17.15	22.7	35.55	14.59	25.38	38.78	11.08	18.02	27.83	11.4
ASTGCN(r)	17.69	29.66	19.4	22.93	35.22	16.56	28.05	42.57	13.92	18.61	28.16	13.08
STSGCN	17.48	29.21	16.78	21.19	33.65	13.9	24.26	39.03	10.21	19.13	31.05	12.68
STFGNN	16.77	26.28	16.3	20.48	32.51	16.77	23.46	36.6	9.21	17.13	26.8	10.96
AGCRN	15.98	28.25	15.23	19.83	32.3	12.97	22.37	36.55	9.12	16.94	26.25	10.6
SCIInet	15	24.31	14.29	18.95	30.89	11.86	21.19	34.03	8.83	15.72	24.76	9.8
DSTAGNN	15.57	27.21	14.68	19.3	31.46	12.7	21.42	34.51	9.01	15.9	25.24	9.97
IRN	14.98	23.99	14.18	19.03	30.88	11.71	21.11	33.99	8.84	15.71	24.64	9.8

4.2 BASELINES

For each dataset, we compare IRN with the latest baselines: (1) For **ETT**, Transformer-based methods (i.e., LogTrans (Li et al., 2019), Informer (Zhou et al., 2021) Autoformer (Wu et al., 2021), Reformer (Kitaev et al., 2020), TST (Zerveas et al., 2021), and Pyraformer (Liu et al., 2021b)) and feature representation learning based methods (i.e., TCC (Eldele et al., 2021), N-BEATS (Oreshkin et al., 2019), CPC (Oord et al., 2018), Triplet (Franceschi et al., 2019), MoCo (He et al., 2020), TNC (Tonekaboni et al., 2021), TS2Vec (Yue et al., 2022), SCIInet(Liu et al., 2021a) and CoST (Woo et al., 2022)); (2) For **PEMS**, LSTM (Hochreiter & Schmidhuber, 1997), CNN-based methods (i.e., TCN and DCRNN (Li et al., 2017)), SCIInet, Graph-based methods (i.e., STGCN (Yu et al., 2017), ASTGCN(r) (Guo et al., 2019), STSGCN (Song et al., 2020), STFGNN (Li & Zhu, 2021), AGCRN (Bai et al., 2020), and DSTAGNN (Lan et al., 2022)); (3) For **Solar Energy, Traffic, Electricity, and Exchange Rate**, AR, VAR-MLP (Zhang, 2003), GP (Frigola, 2015), GRU, LSTNet (Lai et al., 2018), TPA-LSTM (Shih et al., 2019), SCIInet, and MTGNN (Wu et al., 2020).

4.3 EXPERIMENTAL RESULTS

We summarize the performances of IRN and baseline models in Table 2 to 5. IRN demonstrates state-of-the-art performances in 36 cases and near-best in 14 cases. Autoformer performs better for long-term forecasting in ETTh2 datasets as it shows strengths in reflecting trends and seasonality, which are more apparent in longer sequences (Wu et al., 2021). In a similar vein, features are more

Table 5: Forecasting performance comparison of IRN and baseline models on the Solar-Energy, Traffic, Electricity, and Exchange-rate datasets. Best results are highlighted in bold.

Methods	Metrics	Solar-Energy				Traffic				Electricity				Exchange-rate			
		3	6	12	24	3	6	12	24	3	6	12	24	3	6	12	24
AR	RSE	0.2435	0.379	0.5911	0.8699	0.5991	0.6218	0.6252	0.63	0.0995	0.1035	0.105	0.1054	0.0228	0.0279	0.0353	0.0445
	CORR	0.971	0.9263	0.8107	0.5314	0.7752	0.7568	0.7544	0.7591	0.8845	0.8632	0.8691	0.8595	0.9734	0.9656	0.9526	0.9357
VARMPLP	RSE	0.1922	0.2679	0.4244	0.6841	0.5582	0.6579	0.6023	0.6146	0.1393	0.162	0.1557	0.1274	0.0265	0.0394	0.0407	0.0578
	CORR	0.9829	0.9655	0.9058	0.7149	0.8245	0.7695	0.7929	0.7891	0.8708	0.8389	0.8192	0.8679	0.8609	0.8725	0.828	0.7675
GP	RSE	0.2259	0.3286	0.52	0.7973	0.6082	0.6772	0.6406	0.5995	0.15	0.1907	0.1621	0.1273	0.0239	0.0272	0.0394	0.058
	CORR	0.9751	0.9448	0.8518	0.5971	0.7831	0.7406	0.7671	0.7909	0.867	0.8334	0.8394	0.8818	0.8713	0.8193	0.8484	0.8278
RNN_GRU	RSE	0.1932	0.2628	0.4163	0.4852	0.5358	0.5522	0.5562	0.5633	0.1102	0.1144	0.1183	0.1295	0.0192	0.0264	0.0408	0.0626
	CORR	0.9823	0.9675	0.915	0.8823	0.8511	0.8405	0.8345	0.83	0.8597	0.8623	0.8472	0.8651	0.9786	0.9712	0.9531	0.9223
LSTNet	RSE	0.1843	0.2559	0.3254	0.4643	0.4777	0.4893	0.495	0.4973	0.0864	0.0931	0.1007	0.1007	0.0226	0.028	0.0356	0.0449
	CORR	0.9843	0.969	0.9467	0.887	0.8721	0.869	0.8614	0.8588	0.9283	0.9135	0.9077	0.9119	0.9735	0.9658	0.9511	0.9354
SCInet	RSE	0.1775	0.2301	0.2997	0.4081	0.4216	0.4414	0.4495	0.4453	0.0748	0.0845	0.0926	0.0976	0.018	0.0247	0.034	0.0442
	CORR	0.9853	0.9739	0.955	0.9112	0.892	0.8809	0.8772	0.8825	0.9492	0.9386	0.9304	0.9274	0.9739	0.9662	0.9487	0.9255
TPA-LSTM	RSE	0.1803	0.2347	0.3234	0.4389	0.4487	0.4658	0.4641	0.4765	0.0823	0.0916	0.0964	0.1006	0.174	0.241	0.0341	0.0444
	CORR	0.985	0.9742	0.9487	0.9081	0.8812	0.8717	0.8794	0.8629	0.9439	0.9337	0.925	0.9133	0.979	0.9709	0.9564	0.9381
MTGNN	RSE	0.1778	0.2348	0.3109	0.427	0.4162	0.4754	0.4461	0.4535	0.0745	0.0878	0.0916	0.0953	0.0194	0.0259	0.0349	0.0456
	CORR	0.9852	0.9726	0.9509	0.9031	0.8963	0.8667	0.8794	0.881	0.9474	0.9316	0.9278	0.9234	0.9786	0.9708	0.9551	0.9372
IRN	RSE	0.1770	0.2292	0.2971	0.4050	0.4171	0.4349	0.4493	0.4449	0.0739	0.0844	0.0926	0.0968	0.0179	0.0246	0.0337	0.0441
	CORR	0.9853	0.9853	0.9556	0.9112	0.8920	0.8861	0.8774	0.8788	0.9493	0.939	0.9313	0.9281	0.9765	0.9678	0.9522	0.9288

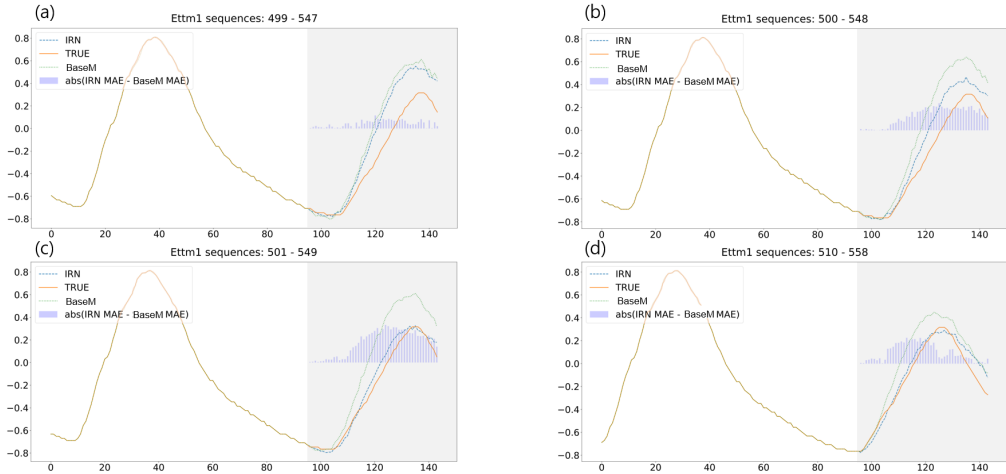


Figure 5: Forecasting results of IRN and the base model from (a) sequence 499 to 547, (b) sequence 500 to 548, (c) sequence 501 to 549, (d) sequence 510 to 558 in ETTm1 data. The ground truths are shown in a solid line. The dotted and dashed lines represent the predicted values of the base model and IRN, respectively. The predicting region is shaded in grey. The bar graph shows the absolute MAE difference between the base model and IRN.

evident in univariate time series, which explains the higher performances of MoCo (He et al., 2020) and CoST (Woo et al., 2022), which are feature representation learning models, on 6 cases of ETT univariate datasets. MTGNN (Wu et al., 2020), a model specialized for analyzing edge relations, yields the best performance on Traffic and Electricity datasets. This is because both datasets contain complex edge between nodes. At last, compared to the attention-based model, IRN shows lesser performances on Exchange-rate dataset due to the strong random-walk property of the time series (Wright, 2008). Overall, our IRN successfully reflects irregularity representation and complements base model to achieve the higher forecasting performances.

4.4 ABLATION STUDY

We perform the ablation study to demonstrate the benefit obtained by IRB. We plot the ground truths and corresponding predictions of IRN and the base model at 499th, 500th, 501th, and 510th sequences of ETTm1 data as shown Figure 5. In Figure 5 (a), the original time series has a peak in the predicting region shaded in grey. Up to sequence 499, IRN and the base model make similar predictions having large errors. When a sequence is added as in the Figure 5 (b), the discrepancy between the ground truth and the predicted values of IRN decreases. With an additional sequence in the Figure 5 (c), IRN quickly reflects the change and makes a better forecast than the base model. It is observed that the base model is less sensitive to the change of the input sequences, giving similar

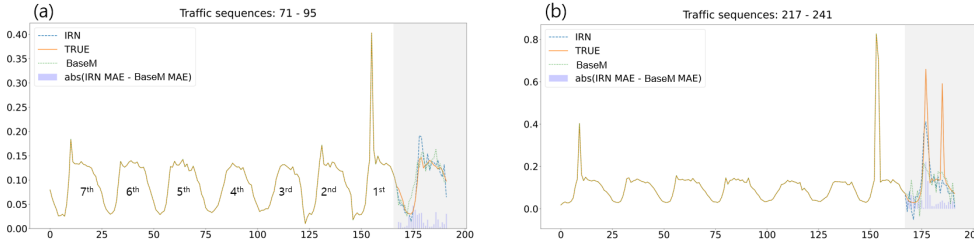


Figure 6: Forecasting results of (a) sequence 71 to 95 and (b) sequence 217 to 241 in traffic data using IRN and base model.

predictions from sequence 499 to sequence 501. Only when 11 sequences have passed, the base model considers the actual changes as in Figure 5 (d). We verify that IRN can reflect the irregular features (instantaneous changes).

Next, we observe the 24 horizon forecasts in Traffic dataset for further analysis. In Figure 6 (a), cycles 2 to 7 consist of values lower than 0.2, whereas cycle 1 includes irregular values greater than 0.3. IRN has larger errors than the base model as IRN instantaneously reflects the irregularity. In contrast, IRN performs better than the base model when the irregularity persists as shown in Figure 6 (b). The reflection of the irregularity does not always end in a better forecast, but IRB consistently improves the forecasting performance of the base model, which confirms the effectiveness of the our model.

4.5 OBSERVATION ON THE VARIATION OF THE IRREGULARITY

We further investigate how the performance of IRN changes with the irregularity of the time series. Ettm1 and Traffic datasets are decomposed into seasonality, trend, and irregularity as depicted in Figure 1. The variation of the irregularity is calculated and classified into two cases according to the degree of variation. Case 1 and Case 2 represent 500 data points with low variation of irregularity and high variation of irregularity, respectively. The difference of average Mean Square Error

Table 6: The difference of average MSE between IRN and base model according to the variation of irregularity on ETTm1 and Traffic datasets. Case 1 and Case 2 refer to 500 data points with low variation in irregularity and with high variation in irregularity, respectively.

Dataset	Horizon	MSE difference between IRN and base model	
		Case 1	Case 2
Ettm1	48	-0.00097	0.001506
Traffic	24	0.00709	0.00941

(MSE) between IRN and base model are obtained for each case and listed in Table 6. This results indicate that higher performance improvement is attained in case 2 than case 1 for both datasets, implying the higher the irregularity variation, the higher performance improvement can be achieved.

5 CONCLUSION

In this paper, we propose Irregularity Reflection Neural Network (IRN), a deep learning based model for time series forecasting that reflects the irregularity in time series. We introduce a novel expression of irregularity based on Fourier series under microscopic perspective condition and employ it to design the Irregularity Representation Block (IRB) that captures, preserves, and learns the irregularity representation of time series data. By embedding the IRB on the base model, IRN is further proposed. Experiments on a variety of real-world datasets show that IRN can consistently outperform existing state-of-the-art baselines. The ablation study confirm that the proposed methodology can reflect the irregularity. Accordingly, we argue that the irregularity representation is essential for improving performance of machine learning models.

REFERENCES

- Sharif Atique, Subrina Noureen, Vishwajit Roy, Vinitha Subburaj, Stephen Bayne, and Joshua Macfie. Forecasting of total daily solar energy generation using arima: A case study. In *2019 IEEE 9th annual computing and communication workshop and conference (CCWC)*, pp. 0114–0119. IEEE, 2019.
- Lei Bai, Lina Yao, Can Li, Xianzhi Wang, and Can Wang. Adaptive graph convolutional recurrent network for traffic forecasting. *Advances in Neural Information Processing Systems*, 33:17804–17815, 2020.
- Peter Bloomfield. *Fourier analysis of time series: an introduction*. John Wiley & Sons, 2004.
- Peter J Brockwell and Richard A Davis. *Time series: theory and methods*. Springer Science & Business Media, 2009.
- Chao Chen, Karl Petty, Alexander Skabardonis, Pravin Varaiya, and Zhanfeng Jia. Freeway performance measurement system: mining loop detector data. *Transportation Research Record*, 1748(1):96–102, 2001.
- Yuxin Chen, Ziqi Zhang, Chunfeng Yuan, Bing Li, Ying Deng, and Weiming Hu. Channel-wise topology refinement graph convolution for skeleton-based action recognition. In *Proceedings of the IEEE/CVF International Conference on Computer Vision*, pp. 13359–13368, 2021.
- Changqing Cheng. Multi-scale gaussian process experts for dynamic evolution prediction of complex systems. *Expert Systems with Applications*, 99:25–31, 2018.
- Junyoung Chung, Caglar Gulcehre, KyungHyun Cho, and Yoshua Bengio. Empirical evaluation of gated recurrent neural networks on sequence modeling. *arXiv preprint arXiv:1412.3555*, 2014.
- Robert B Cleveland, William S Cleveland, Jean E McRae, and Irma Terpenning. Stl: A seasonal-trend decomposition. *J. Off. Stat*, 6(1):3–73, 1990.
- David N DeJong, John C Nankervis, N Eugene Savin, and Charles H Whiteman. Integration versus trend stationary in time series. *Econometrica: Journal of the Econometric Society*, pp. 423–433, 1992.
- Haodong Duan, Yue Zhao, Kai Chen, Dian Shao, Dahua Lin, and Bo Dai. Revisiting skeleton-based action recognition. *arXiv preprint arXiv:2104.13586*, 2021.
- Emadeldeen Eldele, Mohamed Ragab, Zhenghua Chen, Min Wu, Chee Keong Kwoh, Xiaoli Li, and Cuntai Guan. Time-series representation learning via temporal and contextual contrasting. *arXiv preprint arXiv:2106.14112*, 2021.
- Jeffrey L Elman. Finding structure in time. *Cognitive science*, 14(2):179–211, 1990.
- Zheng Fang, Qingqing Long, Guojie Song, and Kunqing Xie. Spatial-temporal graph ode networks for traffic flow forecasting. In *Proceedings of the 27th ACM SIGKDD Conference on Knowledge Discovery & Data Mining*, pp. 364–373, 2021.
- Jean-Yves Franceschi, Aymeric Dieuleveut, and Martin Jaggi. Unsupervised scalable representation learning for multivariate time series. *Advances in neural information processing systems*, 32, 2019.
- Roger Frigola. *Bayesian time series learning with Gaussian processes*. PhD thesis, University of Cambridge, 2015.
- André Gensler, Janosch Henze, Bernhard Sick, and Nils Raabe. Deep learning for solar power forecasting—an approach using autoencoder and lstm neural networks. In *2016 IEEE international conference on systems, man, and cybernetics (SMC)*, pp. 002858–002865. IEEE, 2016.
- Shengnan Guo, Youfang Lin, Ning Feng, Chao Song, and Huaiyu Wan. Attention based spatial-temporal graph convolutional networks for traffic flow forecasting. In *Proceedings of the AAAI conference on artificial intelligence*, volume 33, pp. 922–929, 2019.

- Kaiming He, Xiangyu Zhang, Shaoqing Ren, and Jian Sun. Deep residual learning for image recognition. In *Proceedings of the IEEE conference on computer vision and pattern recognition*, pp. 770–778, 2016.
- Kaiming He, Haoqi Fan, Yuxin Wu, Saining Xie, and Ross Girshick. Momentum contrast for unsupervised visual representation learning. In *Proceedings of the IEEE/CVF conference on computer vision and pattern recognition*, pp. 9729–9738, 2020.
- Sepp Hochreiter and Jürgen Schmidhuber. Long short-term memory. *Neural computation*, 9(8): 1735–1780, 1997.
- Rob J Hyndman and Anne B Koehler. Another look at measures of forecast accuracy. *International journal of forecasting*, 22(4):679–688, 2006.
- Per Jonsson and Lars Eklundh. Seasonality extraction by function fitting to time-series of satellite sensor data. *IEEE transactions on Geoscience and Remote Sensing*, 40(8):1824–1832, 2002.
- Nikita Kitaev, Łukasz Kaiser, and Anselm Levskaya. Reformer: The efficient transformer. *arXiv preprint arXiv:2001.04451*, 2020.
- Guokun Lai, Wei-Cheng Chang, Yiming Yang, and Hanxiao Liu. Modeling long-and short-term temporal patterns with deep neural networks. In *The 41st International ACM SIGIR Conference on Research & Development in Information Retrieval*, pp. 95–104, 2018.
- Shiyong Lan, Yitong Ma, Weikang Huang, Wenwu Wang, Hongyu Yang, and Pyang Li. Dstagnn: Dynamic spatial-temporal aware graph neural network for traffic flow forecasting. In *International Conference on Machine Learning*, pp. 11906–11917. PMLR, 2022.
- Teng-Yok Lee and Han-Wei Shen. Visualization and exploration of temporal trend relationships in multivariate time-varying data. *IEEE Transactions on Visualization and Computer Graphics*, 15(6):1359–1366, 2009.
- Mengzhang Li and Zhanxing Zhu. Spatial-temporal fusion graph neural networks for traffic flow forecasting. In *Proceedings of the AAAI conference on artificial intelligence*, volume 35, pp. 4189–4196, 2021.
- Shiyang Li, Xiaoyong Jin, Yao Xuan, Xiyong Zhou, Wenhui Chen, Yu-Xiang Wang, and Xifeng Yan. Enhancing the locality and breaking the memory bottleneck of transformer on time series forecasting. *Advances in neural information processing systems*, 32, 2019.
- Yaguang Li, Rose Yu, Cyrus Shahabi, and Yan Liu. Diffusion convolutional recurrent neural network: Data-driven traffic forecasting. *arXiv preprint arXiv:1707.01926*, 2017.
- Bryan Lim and Stefan Zohren. Time-series forecasting with deep learning: a survey. *Philosophical Transactions of the Royal Society A*, 379(2194):20200209, 2021.
- Bo Liu, Jianqiang Li, Cheng Chen, Wei Tan, Qiang Chen, and MengChu Zhou. Efficient motif discovery for large-scale time series in healthcare. *IEEE Transactions on Industrial Informatics*, 11(3):583–590, 2015.
- Chengxi Liu, Kenli Li, Jing Liu, and Cen Chen. Lhcnn: A novel efficient multivariate time series prediction framework utilizing convolutional neural networks. In *2019 IEEE 21st International Conference on High Performance Computing and Communications; IEEE 17th International Conference on Smart City; IEEE 5th International Conference on Data Science and Systems (HPCC/SmartCity/DSS)*, pp. 2324–2332. IEEE, 2019.
- Minhao Liu, Ailing Zeng, Zhijian Xu, Qiuxia Lai, and Qiang Xu. Time series is a special sequence: Forecasting with sample convolution and interaction. *arXiv preprint arXiv:2106.09305*, 2021a.
- Shizhan Liu, Hang Yu, Cong Liao, Jianguo Li, Weiyao Lin, Alex X Liu, and Schahram Dustdar. Pyraformer: Low-complexity pyramidal attention for long-range time series modeling and forecasting. In *International Conference on Learning Representations*, 2021b.

- Yeqi Liu, Chuanyang Gong, Ling Yang, and Yingyi Chen. Dstp-rnn: A dual-stage two-phase attention-based recurrent neural network for long-term and multivariate time series prediction. *Expert Systems with Applications*, 143:113082, 2020.
- Spyros Makridakis, Allan Andersen, Robert Carbone, Robert Fildes, Michele Hibon, Rudolf Lewandowski, Joseph Newton, Emanuel Parzen, and Robert Winkler. The accuracy of extrapolation (time series) methods: Results of a forecasting competition. *Journal of forecasting*, 1(2): 111–153, 1982.
- Guido F Montufar, Razvan Pascanu, Kyunghyun Cho, and Yoshua Bengio. On the number of linear regions of deep neural networks. *Advances in neural information processing systems*, 27, 2014.
- Aaron van den Oord, Sander Dieleman, Heiga Zen, Karen Simonyan, Oriol Vinyals, Alex Graves, Nal Kalchbrenner, Andrew Senior, and Koray Kavukcuoglu. Wavenet: A generative model for raw audio. *arXiv preprint arXiv:1609.03499*, 2016.
- Aaron van den Oord, Yazhe Li, and Oriol Vinyals. Representation learning with contrastive predictive coding. *arXiv preprint arXiv:1807.03748*, 2018.
- Boris N Oreshkin, Dmitri Carpov, Nicolas Chapados, and Yoshua Bengio. N-beats: Neural basis expansion analysis for interpretable time series forecasting. In *International Conference on Learning Representations*, 2019.
- Daniele Ravi, Charence Wong, Benny Lo, and Guang-Zhong Yang. A deep learning approach to on-node sensor data analytics for mobile or wearable devices. *IEEE journal of biomedical and health informatics*, 21(1):56–64, 2016.
- Rajat Sen, Hsiang-Fu Yu, and Inderjit S Dhillon. Think globally, act locally: A deep neural network approach to high-dimensional time series forecasting. *Advances in neural information processing systems*, 32, 2019.
- Xingjian Shi, Hourong Chen, Hao Wang, Dit-Yan Yeung, Wai-Kin Wong, and Wang-chun Woo. Convolutional lstm network: A machine learning approach for precipitation nowcasting. *Advances in neural information processing systems*, 28, 2015.
- Shun-Yao Shih, Fan-Keng Sun, and Hung-yi Lee. Temporal pattern attention for multivariate time series forecasting. *Machine Learning*, 108(8):1421–1441, 2019.
- Chao Song, Youfang Lin, Shengnan Guo, and Huaiyu Wan. Spatial-temporal synchronous graph convolutional networks: A new framework for spatial-temporal network data forecasting. In *Proceedings of the AAAI Conference on Artificial Intelligence*, volume 34, pp. 914–921, 2020.
- Donghwan Song, Adrian Matias Chung Baek, and Namhun Kim. Forecasting stock market indices using padding-based fourier transform denoising and time series deep learning models. *IEEE Access*, 9:83786–83796, 2021.
- Sean J Taylor and Benjamin Letham. Forecasting at scale. *The American Statistician*, 72(1):37–45, 2018.
- Sana Tonekaboni, Danny Eytan, and Anna Goldenberg. Unsupervised representation learning for time series with temporal neighborhood coding. *arXiv preprint arXiv:2106.00750*, 2021.
- Mascha Van Der Voort, Mark Dougherty, and Susan Watson. Combining kohonen maps with arima time series models to forecast traffic flow. *Transportation Research Part C: Emerging Technologies*, 4(5):307–318, 1996.
- Kang Wang, Kenli Li, Liqian Zhou, Yikun Hu, Zhongyao Cheng, Jing Liu, and Cen Chen. Multiple convolutional neural networks for multivariate time series prediction. *Neurocomputing*, 360:107–119, 2019.
- Billy M Williams and Lester A Hoel. Modeling and forecasting vehicular traffic flow as a seasonal arima process: Theoretical basis and empirical results. *Journal of transportation engineering*, 129(6):664–672, 2003.

- Gerald Woo, Chenghao Liu, Doyen Sahoo, Akshat Kumar, and Steven Hoi. Cost: Contrastive learning of disentangled seasonal-trend representations for time series forecasting. *arXiv preprint arXiv:2202.01575*, 2022.
- Jonathan H Wright. Bayesian model averaging and exchange rate forecasts. *Journal of Econometrics*, 146(2):329–341, 2008.
- Haixu Wu, Jiehui Xu, Jianmin Wang, and Mingsheng Long. Autoformer: Decomposition transformers with auto-correlation for long-term series forecasting. *Advances in Neural Information Processing Systems*, 34, 2021.
- Zonghan Wu, Shirui Pan, Guodong Long, Jing Jiang, Xiaojun Chang, and Chengqi Zhang. Connecting the dots: Multivariate time series forecasting with graph neural networks. In *Proceedings of the 26th ACM SIGKDD International Conference on Knowledge Discovery & Data Mining*, pp. 753–763, 2020.
- Yongsang Yoon, Jongmin Yu, and Moongu Jeon. Predictively encoded graph convolutional network for noise-robust skeleton-based action recognition. *Applied Intelligence*, 52(3):2317–2331, 2022.
- Bing Yu, Haoteng Yin, and Zhanxing Zhu. Spatio-temporal graph convolutional networks: A deep learning framework for traffic forecasting. *arXiv preprint arXiv:1709.04875*, 2017.
- Zhihan Yue, Yujing Wang, Juanyong Duan, Tianmeng Yang, Congrui Huang, Yunhai Tong, and Bixiong Xu. Ts2vec: Towards universal representation of time series. In *Proceedings of the AAAI Conference on Artificial Intelligence*, volume 36, pp. 8980–8987, 2022.
- George Zerveas, Srideepika Jayaraman, Dhaval Patel, Anuradha Bhamidipaty, and Carsten Eickhoff. A transformer-based framework for multivariate time series representation learning. In *Proceedings of the 27th ACM SIGKDD Conference on Knowledge Discovery & Data Mining*, pp. 2114–2124, 2021.
- G Peter Zhang. Time series forecasting using a hybrid arima and neural network model. *Neurocomputing*, 50:159–175, 2003.
- Pengfei Zhang, Cuiling Lan, Wenjun Zeng, Junliang Xing, Jianru Xue, and Nanning Zheng. Semantics-guided neural networks for efficient skeleton-based human action recognition. In *proceedings of the IEEE/CVF conference on computer vision and pattern recognition*, pp. 1112–1121, 2020.
- Bendong Zhao, Huanzhang Lu, Shangfeng Chen, Junliang Liu, and Dongya Wu. Convolutional neural networks for time series classification. *Journal of Systems Engineering and Electronics*, 28(1):162–169, 2017.
- Haoyi Zhou, Shanghang Zhang, Jieqi Peng, Shuai Zhang, Jianxin Li, Hui Xiong, and Wancai Zhang. Informer: Beyond efficient transformer for long sequence time-series forecasting. In *Proceedings of AAAI*, 2021.

A LOSS FUNCTION

We cover stacked cases in which losses are accumulated. When the dataset has enough training data, we apply K layers (Liu et al., 2021a). To train the K stacked IRN for the k -th intermediate prediction, we compute the L1 loss between the k -th prediction and the true value as follows:

$$L_k = \frac{1}{h} \sum_{i=0}^h |\hat{y}_i^k - y_i|$$

where h is the horizon size, k is the number of stacks, \hat{y}^k is i -th horizon prediction of k -th stack, and y is the true value. We apply Equation 1 to calculate the L1 loss of each stacked layer output. The total loss of the stacked IRN is expressed as:

$$L = \sum_{k=0}^K L_k$$

B IMPLEMENTATION DETAILS

Our model and framework are implemented with Pytorch. We train IRN with Adam optimizer by using NVIDIA 2080Ti 8 GPUs for enough batch size. Other parameters such as learning rate, level, stack, single, and multi are changed according to the dataset characteristics and referring base model (Liu et al., 2021a).

C DATASETS AND METRICS

C.1 ELECTRICITY TRANSFORMER TEMPERATURE

ETT contains two-year electric power data gathered from two counties in China (hourly subsets ETTh1, ETTh2 and 15 minutes subsets ETTm1). Each data point contains an oil temperature value and six power load components. The train, validation and test sets consist of 12, 4, and 4 months data, respectively. We implement zero-mean normalization for data pre-processing. Mean Absolute Errors (MAE) (Hyndman & Koehler, 2006) and Mean Squared Errors (MSE) (Makridakis et al., 1982) are used as evaluation metrics.

$$MAE = \frac{1}{h} \sum_{i=0}^h |\hat{x}_i - x_i|$$

$$MSE = \frac{1}{h} \sum_{i=0}^h (\hat{x}_i - x_i)^2$$

where x_i is the true value, \hat{x}_i is the predicted value, and h is the prediction horizon size.

C.2 PEMS

PeMS consists of four public datasets (i.e., PEMS03, PEMS04, PEMS07 and PEMS08), which are separately collected from Caltrans Performance Measurement System (PeMS) of four sections in California. The data is collected every five minutes. We predict one hour that consists of 12 data points. The zero-mean normalization is applied for the data pre-processing. The evaluation metrics are MAE, Root Mean Squared Errors (RMSE) and Mean Absolute Percentage Errors (MAPE).

$$RMSE = \sqrt{\frac{1}{h} \sum_{i=0}^h (\hat{x}_i - x_i)^2}$$

$$MAPE = \frac{1}{h} \sum_{i=0}^h \left| \frac{\hat{x}_i - x_i}{x_i} \right|$$

C.3 TRAFFIC, SOLAR ENERGY, ELECTRICITY AND EXCHANGE RATE

Traffic includes the hourly road occupancy rates which ranges from 0 to 1. The sensors gather the road occupancy rates from 2015 to 2016. Solar Energy contains 2016 solar power production which are recorded every 10 minutes from 137 PV plants in Alabama State. Electricity collects the hourly electricity consumption (kWh) of 321 clients from 2012 to 2014. Exchange-Rate consists of the daily exchange rates of 8 foreign countries from 1990 to 2016. For four datasets, the size of the lookback window is 168, and horizon sizes are 3,6,12, and 24. The evaluation metrics are Root Relative Squared Error (RSE) and Empirical Correlation Coefficient (CORR) (Lai et al., 2018).

$$RSE = \frac{\sqrt{\sum_{i=0}^h (\hat{x}_i - x_i)^2}}{\sqrt{\sum_{i=0}^h (x_i - \text{mean}(x))^2}}$$

$$CORR = \frac{1}{d} \sum_{j=0}^d \frac{\sum_{i=0}^h (x_{i,j} - \text{mean}(x_j))(\hat{x}_{i,j} - \text{mean}(\hat{x}_j))}{\sum_{i=0}^h (x_{i,j} - \text{mean}(x_j))^2 (\hat{x}_{i,j} - \text{mean}(\hat{x}_j))^2}$$

where d is the number of variates.